BULLETIN OF THE POLISH ACADEMY OF SCIENCES
TECHNICAL SCIENCES,
DOI:10.24425/bpasts.2026.158773

Modelling of a Five-Phase Induction Motor with Quasi-Trapezoidal Air-Gap Flux Density Distribution

Krzysztof Blecharz[1]*, **Roland Ryndzionek**[1]

[1] Gdansk University of Technology, Faculty of Electrical and Control Engineering, Narutowicza Street 11/12, 80-233 Gdansk, Poland

Abstract. This article proposes a practical and flexible modelling approach for a five-phase squirrel-cage induction motor that explicitly accounts for the shape of the air-gap magnetic flux density distribution. Two motor configurations are analysed and compared: one with a sinusoidal air-gap flux distribution and another with a quasi-trapezoidal distribution obtained through third-harmonic voltage injection. The proposed modelling framework is based on vector space decomposition into two orthogonal mathematical planes and is implemented using standard components available in the PLECS simulation environment. Finite element analysis is used to support the selection of model parameters and to evaluate the influence of harmonic injection on the air-gap flux distribution. The developed models are verified by simulations and laboratory experiments carried out on the five-phase induction motor. The results confirm that a quasi-trapezoidal air-gap flux distribution enables the second vector plane to contribute to torque production and leads to improved magnetic flux utilisation. The proposed approach provides a clear and flexible tool for the analysis and development of control strategies for five-phase induction motor drives.

Key words: five-phase induction motor; multi-phase motor; simulation software;

1. INTRODUCTION

Multiphase induction machines represent an alternative to conventional three-phase squirrel-cage motors, particularly in applications where additional degrees of freedom in machine operation are of interest. As widely reported in the literature, such machines allow torque enhancement through harmonic-assisted operation and can maintain electromagnetic torque under phase deactivation, providing increased operational robustness in selected applications. This enhances the reliability of the motor's performance in specific high-demand applications [1–3].

A scalar or vector control scheme for a five-phase machine is fundamentally similar to the corresponding scheme for a classic three-phase induction motor [4,5]. In order to achieve complete control of the machine for decoupled flux and torque control in a squirrel-cage motor using the vector control method, it is necessary to regulate the stator current components in the d-q two-axis reference frame. In multiphase motors, the number of phases has a direct impact on the design of the control algorithm, offering increased flexibility in the machine's mathematical model. This, in turn, facilitates the development of novel control structures. Utilising the two additional degrees of freedom available in a five-phase machine allows for the achievement of a higher electromagnetic torque density. Moreover, the integration of a third stator current harmonic into the machine's operations facilitates the exploitation of the third spatial harmonic of the field for torque production, complementing the fundamental harmonic of field production [6].

The control system has been developed to allow for independent regulation of the 1^{st} and 3^{rd} stator voltage harmonic components. It can thus be concluded that two synchronised voltage sources are required for the generation of the stator voltage component $u_{s\alpha}, u_{s\beta}, u_{sx}, u_{sy}$ for each mathematical plane in an orthogonal frame, in order to implement a 3^{rd} harmonic injection drive.

Research on multiphase machines is focused in two key areas. Firstly, the initial domain encompasses the design and development of the machines themselves, incorporating the configuration of windings on both the stator and rotor sides [7, 8] and the design and optimisation of the machines' magnetic circuits [9–11]. The present study employs computer programmes that utilise the finite element method. Secondly, the research focuses on the further development of control methodologies [12–15]. A significant research direction in the area of control methods is the development of control algorithms that utilise the motor's ability to operate in both mathematical planes. This enables an increase in electromagnetic torque of several per cent, facilitates enhanced utilisation of the machine's magnetic circuit, and leads to a reduction in internal losses. Moreover, the control methods implemented are capable of managing the operational and emergency states of the drive system. This includes scenarios such as a loss of power in one or two non-adjacent phases of the motor stator circuit [16]

Commercial and open-source simulation tools such as MATLAB/Simulink, PLECS, Altair PSIM, and Scilab/Xcos or OpenModelica are currently being used to develop control and regulation systems for electric drives. These programmes are the primary tools employed by numerous research teams for the purpose of simulating drive and power-electronics systems. Furthermore, due to their flexibility, ease of use and accessibility, they are widely used in education and student training. Unfortunately, with the growing interest in multiphase machines and drive systems, there has been a difficulty for users to access models of multiphase induction and permanent-magnet machines. The absence of custom models for electric machine

*e-mail: krzysztof.blecharz@pg.edu.pl

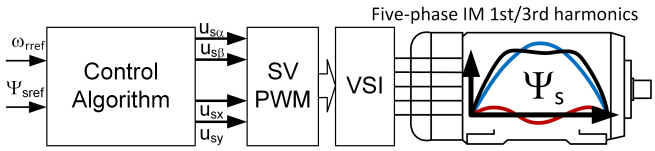

Fig. 1. Schematic diagram of the drive system with five-phase induction motor

designs poses a significant challenge for research teams. However, simulation programs provide the functionality to incorporate a block or blocks of functional code containing C++ code into the model. This model may be of the entire drive system. This functionality facilitates the representation of any model of the multiphase machine under investigation through the utilisation of differential equations. Despite the fact that the proposed solution is highly flexible and functional, it has several disadvantages. Descriptive code is less legible than the structure of a simulation model in block diagram form. Furthermore, documenting code changes in collaboration with larger, multinational research teams is also challenging. A significant problem is the potential for, and the occurrence of, hard-to-detect programming errors in the code, such as implicit type conversions. Moreover, the utilisation of functional blocks with C++ code necessitates manual management of the I/O interface, a factor which has the potential to result in the occurrence of additional errors.

This article presents and discusses a methodology for modelling a five-phase induction motor, with particular emphasis on the differences between machine designs featuring sinusoidal and quasi-trapezoidal air-gap magnetic flux density distributions. The general structure of the drive system has been presented in Fig. 1. It is demonstrated that the shape of the air-gap flux distribution has a direct impact on the electromagnetic behaviour of the machine, determining whether the second vector plane contributes to torque production, which occurs only in the case of a quasi-trapezoidal distribution. Based on this physical observation, two corresponding universal equivalent-circuit models are formulated, reflecting the different roles of the second plane in the overall torque-generation mechanism. The proposed models are implemented using standard simulation blocks in the PLECS environment and are evaluated through a series of time-domain simulation studies. The validity of the modelling approach is further confirmed by laboratory measurements performed under both steady-state and dynamic operating conditions.

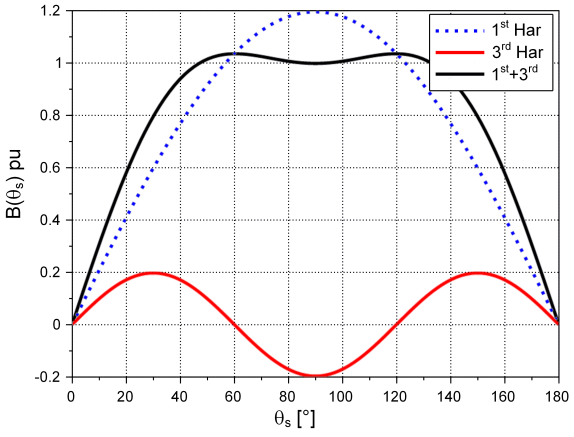

Fig. 2. Stator flux density distribution and its components.

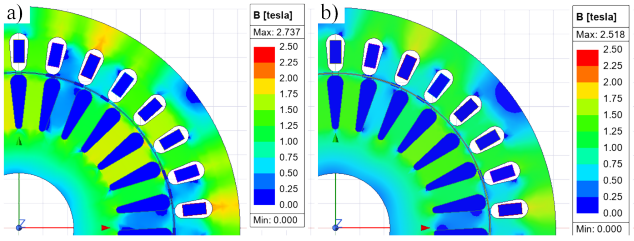

Fig. 3. Flux density distribution for 5FIM a) only fundamental, b) with quasi-trapezoidal distribution

2. FIVE-PHASE MOTOR WITH QUASI-TRAPEZOIDAL AIR-GAP FLUX DENSITY DISTRIBUTION

Significant features that increase the usefulness of the five-phase induction motor drives compared to three-phase induction motor drives include greater fault tolerance for the loss of one or two stator phases and the ability to generate an additional electromagnetic torque component with appropriate system control [17, 18]. The two-dimensional transient finite element method (2D-TFEM) is utilised to ascertain the performance of the multiphase IM. The merits of the finite element method (FEA) are predicated on its ability to comprehensively and accurately simulate the realistic conditions of geometries, core materials and winding connections. Furthermore, the effective shaping of the magnetic flux distribution within the machine's air gap is a critical factor in determining the magnitude of the additional torque component generated by the provision of the motor with a third-harmonic current. In contrast to the conventional approach to three-phase motor design, which necessitates a sinusoidal distribution of induction in the machine's air gap, achieving a quasi-trapezoidal distribution is particularly advantageous in five-phase motors (Fig. 2). This approach enables the enhancement of machine efficiency through the reduction of magnetic-circuit losses, a significant consequence of these choices [19].

Simulation results for a cross-section of a 5PIM motor developed in Ansys Maxwell software. The stator winding was designed as a single-layer 5-phase winding with 3-pole pairs; the stator and rotor slots are 30 and 27, respectively. The rotor winding is a squirrel-cage winding. The rotor has been modelled with the appropriate core skew. This is necessary to eliminate the influence of higher harmonics in the results and to obtain the quasi-trapezoidal flux distribution.

The simulation results are shown in Fig. 3. The simulation was performed for the same load conditions, but with a different voltage supply source. Fig. 3a shows the supply voltage only with the amplitude of the fundamental harmonic, while Fig. 3b shows the fundamental voltage with an additional third

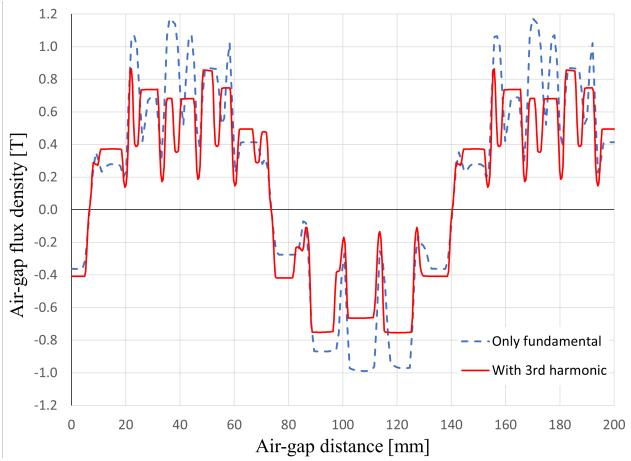

Fig. 4. Air-gap flux density distribution. The blue dashed line is only flux density with amplitude of fundamental harmonic, red line is flux density with additional third harmonic.

harmonic with an amplitude of 30% of the fundamental. As can be seen, for equivalent operating conditions, the maximum amplitude (in stator core) of flux density is substantially lower for the quasi-trapezoidal distribution (from 15-20% of the maximum value).

The distribution of flux density in the air gap has also been investigated (Fig. 4). As demonstrated, incorporating the third harmonic leads to a reduction in the flux and consequently generates a more uniform distribution of induction within the air-gap. The maximum amplitude of air-gap flux density is approximately 1.2 T and 0.8 T for only fundamental and 3rd harmonic, respectively. Moreover, the higher harmonics of the air gap flux density in five-pole phase conditions are negligible and thus do not exert any discernible influence on the performance of the 5PIM.

The FEA simulation results are of particular importance, as they provide information on motor parameters that are otherwise difficult to measure. The results of the simulations provide a foundation for the configuration and synthesis of an equivalent circuit for a multiphase machine in a dual mathematical plane.

3. VECTOR MODELS OF FIVE-PHASE INDUCTION MOTOR

The development of a simulation model of a five-phase induction motor, in the form of a functional block for use in a simulation program, is predicated on a comprehensive understanding of the motor's internal structure, as well as the properties of multiphase systems themselves. The system under discussion comprises two model variants. The initial variant pertains to a motor design characterised by a quasi-trapezoidal flux distribution within the air gap, while the subsequent variant involves a design with a sinusoidal field distribution. The design of both motors is based on mathematical relationships that have been documented in the literature [20]. A key feature of symmetrical five-phase systems in natural axes during the transition to an orthogonal system, facilitated by the Park transform, is the ability to express the model in two decoupled systems of orthogonal reference frames. The five-phase induction motor can be represented as two independent virtual machines [21] supplied by a single five-phase voltage or current source. A common drive shaft physically connects these machines.

The generator vector model is based on several standard assumptions: the magnetic circuit is linear and magnetic saturation is not included, the winding distribution depends on motor configuration and is assumed to be sinusoidal for the first model or quasi-trapezoidal in the second model, all model parameters are assumed fixed, the air-gap is uniform, and mechanical losses are not considered.

The general form of the vector model of a five-phase induction motor, with standard simplifying assumptions, is:

$$\mathbf{u}_s^{(i)}=\mathbf{R}_s^{(i)}\mathbf{i}_s^{(i)}+\frac{\mathrm{d}\Psi_s^{(i)}}{\mathrm{d}t}+\mathrm{j}\omega_\mathrm{a}\Psi_s^{(i)}, \tag{1}$$

$$0=\mathbf{R}_r^{(i)}\mathbf{i}_r^{(i)}+\frac{\mathrm{d}\Psi_r^{(i)}}{\mathrm{d}t}+\mathrm{j}\left(\omega_\mathrm{a}-\omega_r^{(i)}\right)\Psi_r^{(i)}, \tag{2}$$

flux equations are defined as:

$$\Psi_s^{(i)}=\mathbf{L}_s^{(i)}\mathbf{i}_s^{(i)}+\mathbf{L}_m^{(i)}\mathbf{i}_r^{(i)}, \tag{3}$$

$$\Psi_r^{(i)}=\mathbf{L}_r^{(i)}\mathbf{i}_r^{(i)}+\mathbf{L}_m^{(i)}\mathbf{i}_s^{(i)}. \tag{4}$$

where $\Psi_s^{(i)},\mathbf{i}_s^{(i)},\mathbf{u}_s^{(i)}$ and $\Psi_r^{(i)},\mathbf{i}_r^{(i)}$ are the stator and rotor space vectors of magnetic fluxes, circuit currents and voltage for each mathematical plane, respectively. The dynamics of the mechanical part of the model are described by the equation in which the electromagnetic moment is the sum of moments arising from components defined on individual mathematical planes. The general form of the equation is as follows:

$$\mathrm{J}\frac{d\omega_r}{dt}=\frac{5}{2}\mathrm{p}\sum_{i=1}^{2}\mathrm{Im}\left|\Psi_\mathrm{s}^{(\mathrm{i})*}\ \mathbf{i}_\mathrm{s}^{(\mathrm{i})}\right|-\mathrm{T}_{load} \tag{5}$$

where J is the rotor moment of inertia, p is number of pole pairs, and T_{load} is load torque. The superscript (i = 1..2) defines sets of state variable equations for two independent mathematical planes of state variables 1 and 2. The components of the machine model variable vectors on the first mathematical plane are designated $(\alpha-\beta)$, while on the second plane they correspond to the designation $(x-y)$. The superscript also corresponds to the parameters of the motor model, which, depending on the internal design, may differ for each plane considered.

The inductance of stator, rotor and mutual inductance, denoted as $L_s^{(i)}, L_r^{(i)}$, and $L_m^{(i)}$, also require indexing due to the two mathematical planes that exist:

$$L_s^{(i)}=L_{\sigma 2}^{(i)}+L_m^{(i)}, \qquad L_r^{(i)}=L_{\sigma 2}^{(i)}+L_m^{(i)} \tag{6}$$

The control system used to utilize the features of the second-math plane 3^{rd}- harmonic injection is described in the literature [21]. An orthogonal plane that rotates three times faster and in the opposite direction to the fundamental is required to take advantage of the 3^{rd} harmonic, therefore

$$\omega_r^{(2)} = -3\omega_r^{(1)} \tag{7}$$

The electric motor model equations in the form (1) - (5) are general relations that can be written in two ways, depending on the adopted simplifying assumptions. Assuming the rotational speed of the reference system, ω_a, is equal to zero, the system is stationary with respect to the machine stator. In the first case, for a motor design with a quasi-trapezoidal air-gap flux distribution, the set of equations takes the form for the first plane $(\alpha-\beta)$:

$$\frac{d\Psi_{s\alpha}}{dt} = -R_s^{(1)} i_{s\alpha} + u_{s\alpha}, \qquad \frac{d\Psi_{s\beta}}{dt} = -R_s^{(1)} i_{s\beta} + u_{s\beta} \tag{8}$$

$$\frac{d\Psi_{r\alpha}}{dt} = -\mathrm{R}_r^{(1)} i_{r\alpha} + \omega_r^{(1)} \Psi_{r\beta}, \qquad \frac{d\Psi_{r\beta}}{dt} = -\mathrm{R}_r^{(1)} i_{r\beta} - \omega_r^{(1)} \Psi_{r\alpha} \tag{9}$$

and for the second plane $(x-y)$:

$$\frac{d\Psi_{sx}}{dt} = -R_s^{(2)} i_{sx} + u_{sx}, \qquad \frac{d\Psi_{sy}}{dt} = -R_s^{(1)} i_{sy} + u_{sy} \tag{10}$$

$$\frac{d\Psi_{rx}}{dt} = -R_r^{(2)} i_{rx} + \omega_r^{(2)} \Psi_{ry}, \qquad \frac{d\Psi_{ry}}{dt} = -R_r^{(2)} i_{ry} - \omega_r^{(2)} \Psi_{rx} \tag{11}$$

The dynamics of the mechanical part of the model are as follows:

$$\begin{aligned} J\frac{d\omega_r^{(1)}}{dt} = \frac{5}{2} p [& \frac{L_m^{(1)}}{L_r^{(1)}} (\Psi_{r\alpha} i_{s\beta} - \Psi_{r\beta} i_{s\alpha}) \\ & + \frac{L_m^{(2)}}{L_r^{(2)}} (\Psi_{rx} i_{sy} - \Psi_{ry} i_{sx})] - T_{load} \end{aligned} \tag{12}$$

In the second case, corresponding to a sinusoidal air-gap flux distribution, the model structure in the second plane is simplified. The vector of the stator magnetic flux generated in the second plane is as follows:

$$\Psi_s^{(2)} = \mathbf{L}_{s\sigma}^{(2)} \mathbf{i}_s^{(2)} \tag{13}$$

hence the dynamic of stator flux equation (1) for second plane for vector components takes the form

$$\frac{d\Psi_{sx}}{dt} = -\frac{R_s^{(2)}}{L_{s\sigma}^{(2)}} \Psi_{sx} + u_{sx}, \qquad \frac{d\Psi_{sy}}{dt} = -\frac{R_s^{(2)}}{L_{s\sigma}^{(2)}} \Psi_{sy} + u_{sy}. \tag{14}$$

In a machine with a sinusoidal air-gap flux distribution, the subsystem in the second mathematical plane $(x-y)$ does not generate an additional electromagnetic torque component. The dynamics of the motor's mechanical part for this configuration take the form:

$$J\frac{d\omega_r^{(1)}}{dt} = \frac{5}{2} p \frac{L_m^{(1)}}{L_r^{(1)}} (\Psi_{r\alpha} i_{s\beta} - \Psi_{r\beta} i_{s\alpha}) - T_{load} \tag{15}$$

For the selected air-gap flux distribution, quasi-trapezoidal or sinusoidal electric motor type, based on the system of equations (8) - (11) or the system of equations (8) - (9) and (14), respectively, two equivalent circuits to the five-phase induction motor model in a stationary reference frame can be created, as shown in Fig. 6.

The blue frame surrounds the equivalent motor circuit defined for the first mathematical plane, while the red frame indicates the equivalent circuit for the second plane. The difference between the models occurs only on the second plane.

4. SIMULATION MODELS OF MOTOR

A top-level diagram of an electric drive model with a five-phase induction motor is shown in Fig. 5. The power stage of the five-phase voltage source inverter (VSI) consists of 10 power switches. Control pulses from the SVPWM block control the IGBT transistors. This block implements the space vector pulse-width modulation (SVPWM) algorithm. The two outputs (1)(2) of this block are vectors with transistor states for the upper and lower positions. The required input voltage vectors' lengths $(|Us1|)$, $(|Us3|)$ and pulsations (omega1), (omega3) for both mathematical planes are calculated in the master control system block, where any user-selected control algorithm can be implemented based on the selected control method. In the described simulation configuration, scalar control was used, which was presented in the publication [22]. To simplify the entire drive model, the rectifier module was replaced with an equivalent constant-voltage source Vi with Vdc = 560 V, which supply the VSI system.

The motor model, which is comprised of five phases, was constructed exclusively using standard functional blocks from the programme's component library. The approach to electric motor modelling was intended to maximise the clarity of the model's structure and ensure consistency and coherence among the various components.

The internal structure of the functional five-phase motor block (5-phase IM) is shown in Fig. 7. The internal structure of the model is determined by the physical internal structure of the magnetic circuits and the topology of the motor windings. The presented motor model considers two solutions: one with a sinusoidal and the other with a quasi-trapezoidal flux density distribution in the air-gap.

The machine model is divided into two subsystems corresponding to the first mathematical plane, marked $(\alpha-\beta)$ in a blue frame, and the second mathematical plane, marked $(x-y)$ in a red frame.

The internal configuration of the motor's equivalent circuit diagram on the first mathematical plane is the same in both motor designs (blue frame). The fundamental difference in the model configuration concerns the construction of the equivalent circuit diagram on the second mathematical plane (red frame), which depends on the shape of the magnetic flux density distribution in the motor's air gap. The differences in the internal structure are shown in Fig. 7: A - sinusoidal distribution, B - quasi-trapezoidal distribution. In the green frame, the mechanical part of the model was marked. This part is identi-

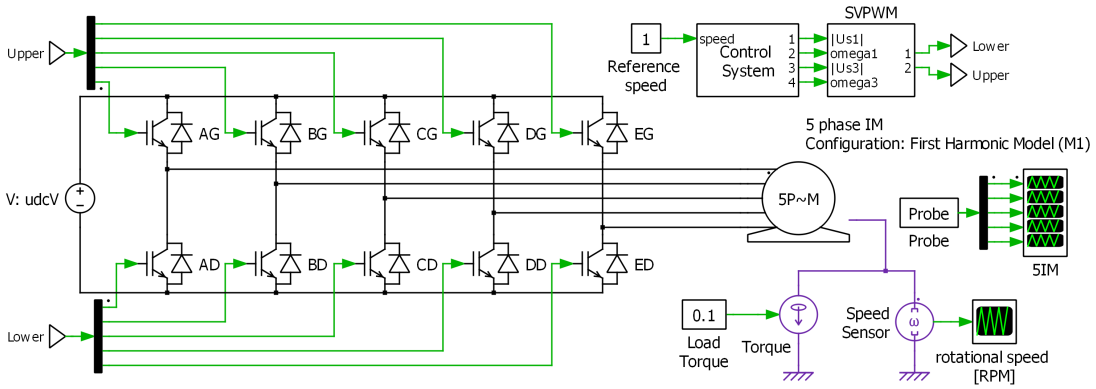

Fig. 5. Schematic diagram of the simulation drive system with a five-phase induction motor.

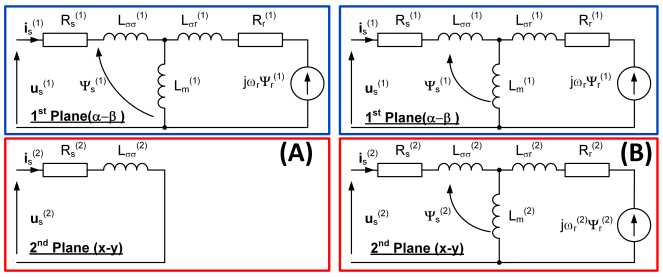

Fig. 6. Equivalent circuits of the five-phase induction motor: A) with sinusoidal distribution, B) with quasi-trapezoidal distribution

cal for both configurations.

A major difficulty in modeling drive systems of multi-phase machines is the connection of the part containing the regulated source in the form of a converter in a natural five-phase system. Transformation functional block (abcde<->alpha-beta-xy) for connecting a five-phase system with two independent orthogonal subsystems with equivalent circuits of motor model for the first and second mathematical planes. The internal structure of the transformation block, which is crucial to the simulation's functionality, is shown in Fig. 8.

Five ideal multi-winding transformers were used to transform the machine's phase currents and voltages between the natural five-phase symmetrical axis system and two orthogonal systems representing the machine model. The five-transformer connection configuration, along with four controlled current sources (Id1-Id4) and four controlled voltage sources (V1-V4) (two controlled sources per independent mathematical plane of the model), allows coupling the five-phase system with the orthogonal alpha-beta and x-y axes system. The transformer ratios of the individual transformers correspond to the coefficients of invert Park's transformation matrix for the five-phase system, consistent with formula (16).

The machine model is based on a four-controlled-current-source implementation at the stator terminals, which connect to the voltage-source inverter. Problems may occur during periods of inactivity in the inverter transistors, due to a shift in the current flow direction between the transistor and the bypass diode. In order to eliminate potential problems during the selected operating states of electric drives, it is necessary to add snubber resistors R1-R4 in parallel with the current sources.

5. SIMULATION STUDIES AND LABORATORY TESTS

In order to verify the correctness of the developed motor model structure and its operation, standard simulation tests were performed, and the results were verified against measurements on a test stand. The drive system was implemented on the PLECS simulation platform, which is designed for power electronics and electric drive systems. Tests of the drive system were conducted in a laboratory setting using a stand that housed a two-level bidirectional power electronic converter rated at 11kW. This converter was controlled by a controller board that incorporated a Sharc ADSP21363 floating-point signal processor and an Altera Cyclone II FPGA. The stand facilitates comprehensive access to all level converter configurations. The PWM switching frequency was 3.3 kHz. The control algorithm code was written in C++ using rules consistent with the processor type. The interrupt time was set to 150μs. Phase currents measurements were obtained using a Tektronix MSO46 multi-channel oscilloscope with current probes. In the laboratory tests, a five-phase squirrel-cage motor with a power rating of 5.5 kW was used. The parameters of the induction motor prototype for the first and second mathematical planes are presented in Table I in Appendix I.

The results obtained from both the simulation and measurement processes are presented successively. The drive system was regulated through the implementation of an open-loop scalar control method, thereby ensuring the maintenance of a constant ratio between the stator voltage, first-harmonic amplitude, and frequency.

In the control system, it is assumed that the 3rd-harmonic component of the stator voltage does not exceed 30% of the fundamental harmonic of the inverter-generated voltage. Fig. 9 illustrates the motor's steady-state operation without a load, while the corresponding measurement results are shown in Fig. 10. Additionally, the phase current waveform obtained from the FEM analysis is shown in the white box.

The next step, the motor was started at 750 rpm. In all test cases, the required stator voltage pulsation was applied using a 1-second ramp. The simulation results are shown in Fig. 11. Fig. 12 shows the current oscillograms corresponding to the

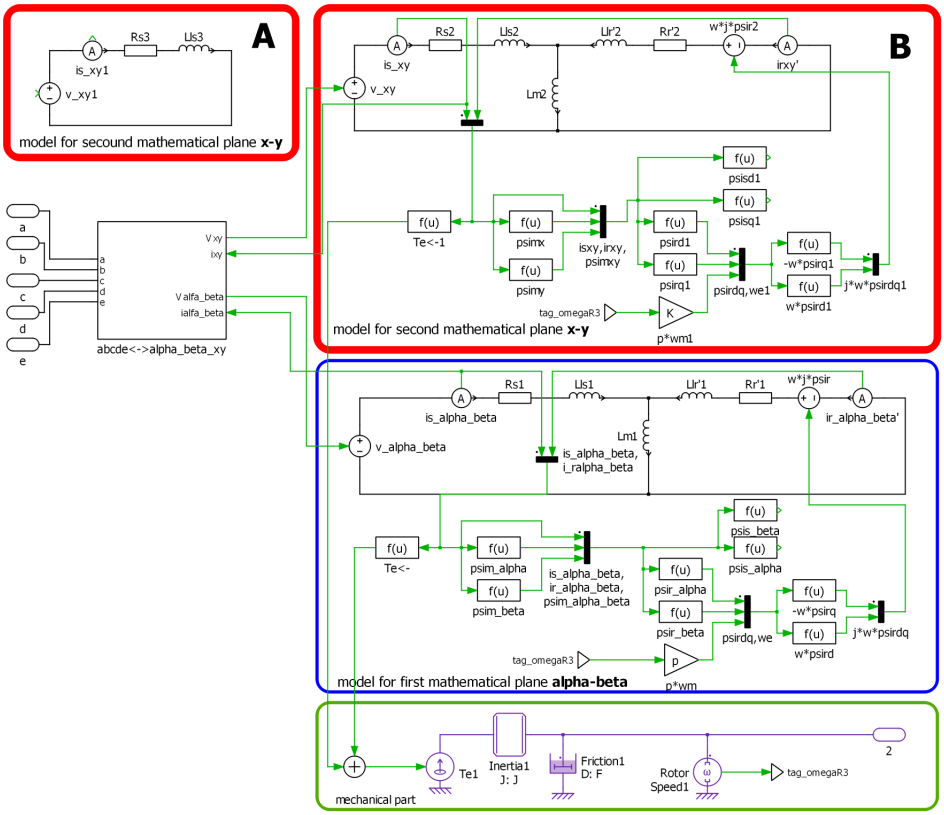

Fig. 7. The two versions of the equivalent circuits of a five-phase induction motor machine in the PLECS software using only standard components: (A)-sinusoidal flux distribution, (B)-quasi-trapezoidal flux distribution.

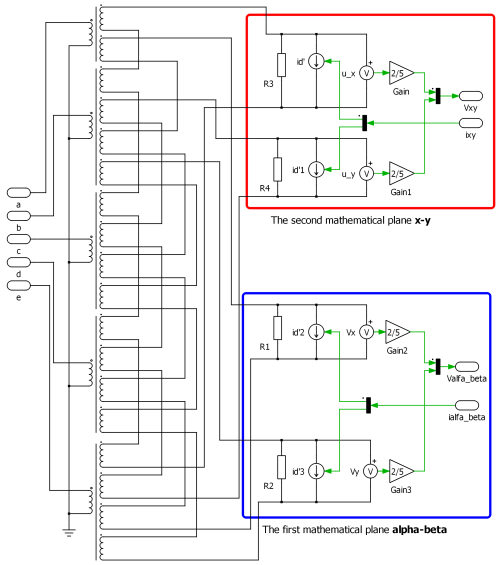

Fig. 8. The structure of a transformation block that is an element connecting a five-phase power supply system with five-phase motor equivalent circuit systems in orthogonal coordinate systems.

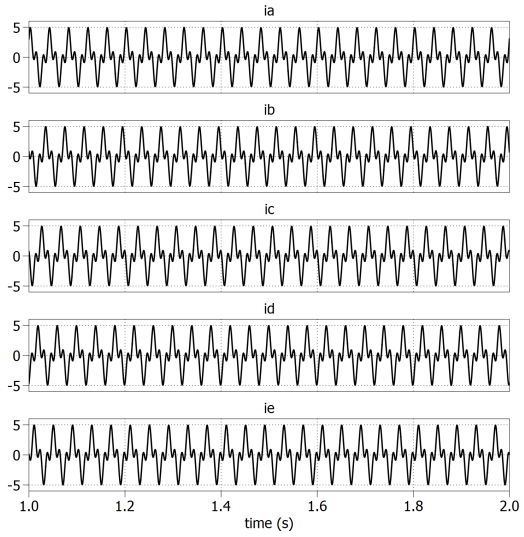

Fig. 9. Stator current waveforms for the steady-state of the machine, simulation results.

motor start procedure. The next test involved forcing the motor shaft rotation direction to change in the drive system model. The test was conducted for a speed range of 750 to -750 rpm. The simulation results are shown in Fig. 13. The measured stator current values are shown in Fig. 14.

The laboratory test results show that the developed model is reliable under both static and dynamic conditions, and third harmonic injection can result in an additional torque component.

It has been demonstrated that the reliability of the measure-

ments and simulations provides substantiated evidence that validates the model's capacity to facilitate the design and evaluation of control algorithms prior to their actual implementation within authentic systems.

6. CONCLUSIONS

This article presents a modelling approach for a five-phase induction motor that accounts for the magnetic flux distribution in the machine's air gap. The injection of the third harmonic into the stator voltage exerts a substantial influence on the distribution of induction in the air gap and the operating parameters of a five-phase induction motor. The model configuration considers two cases: one with a sinusoidal magnetic flux distribution and one with a quasi-trapezoidal distribution.

The models were developed using dual-plane vector representation and implemented with standard components in the PLECS simulation environment. Finite element analysis was used to evaluate the influence of third-harmonic injection on the air-gap flux distribution. The results showed that introducing the third harmonic leads to a more uniform flux distribution and reduced peak flux density, which improves magnetic circuit utilisation without changing the machine geometry. These observations provided the basis for selecting different model structures for the analysed configurations.

Laboratory tests verified the simulation studies on the five-phase motor with a quasi-sinusoidal air-gap field distribution. A comparative analysis of the obtained test results indicates that the motor model, constructed from standard components of the PLECS symbol library, based on a set of mathematical equations (1) - (5), provides an excellent basis for developing and examining control structures for five-phase motors. Moreover, these results confirm that the use of a quasi-trapezoidal induction distribution in combination with third harmonic injection is a beneficial solution in the design of five-phase electric drives, especially in applications requiring high efficiency and overload resistance.

Finally, the present study proposes and validates two structurally distinct models for sinusoidal and quasi-trapezoidal flux distributions. These models demonstrate that a single universal dual-plane model is sufficient for simulating five-phase induction motors. The proposed approach provides a clear and practical framework for modelling and analysing five-phase drives, and can be effectively used in the development and evaluation of control algorithms.

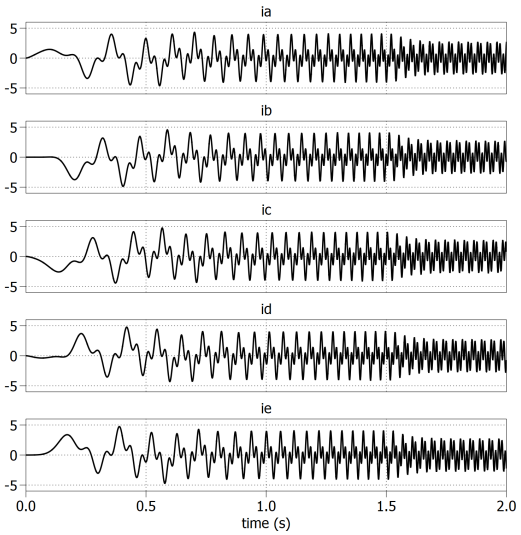

Fig. 11. Transient motor currents for start-up procedure to 750 RPM, simulation results.

ACKNOWLEDGEMENTS

This work was supported by IDUB Ventus-Hydrogenii Gdańsk Tech Program (Grant no. DEC-3/2022/IDUB/VHR), Poland.

APPENDIX

Table 1 presents the parameters of the prototype of a 5-phase induction motor used for laboratory tests. Fig. 15 shows a configuration of the laboratory setup with the analysed 5-phase motor coupled with three 3-phase load motors. The prototype of a 5-phase voltage source inverter supplies the analysed 5-phase induction motor in an electric drive shaft.

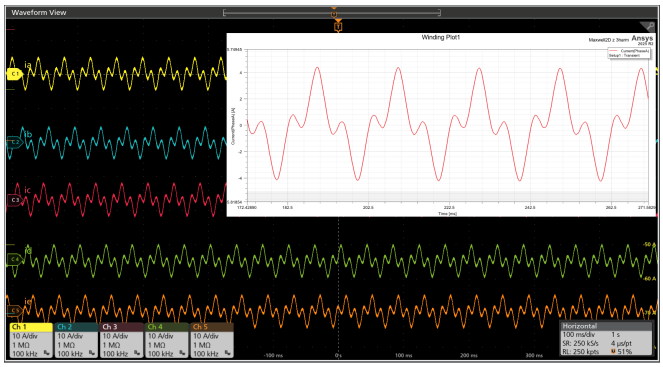

Fig. 10. Stator current waveforms for the steady-state of the machine and FEA results of stator current single phase.

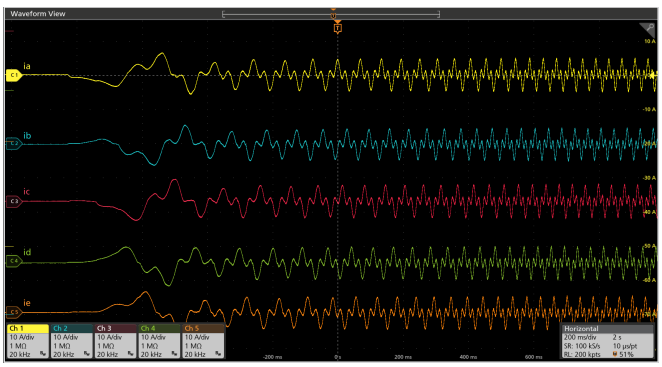

Fig. 12. Transient motor currents for starting procedure up to 750 rpm, measured results.

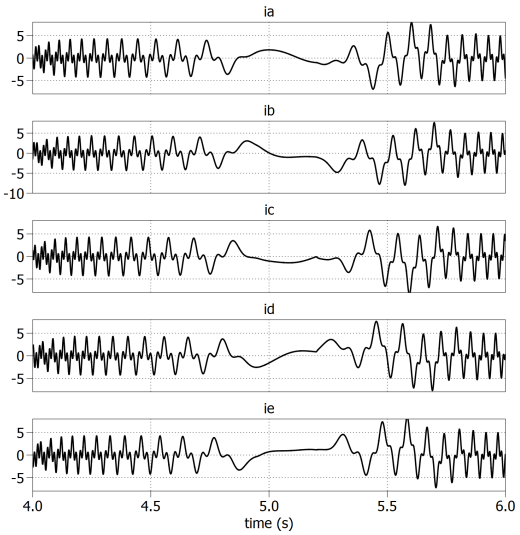

Fig. 13. Stator current waveform for motor reversal procedure in the range of 750 to -750 rpm, simulation results.

$$\begin{bmatrix} i_{sa} \\ i_{sb} \\ i_{sc} \\ i_{sd} \\ i_{se} \end{bmatrix} = \begin{bmatrix} 1 & 0 & 1 & 0 \\ \cos\gamma & \sin\gamma & \cos 2\gamma & \sin 2\gamma \\ \cos 2\gamma & \sin 2\gamma & \cos 4\gamma & \sin 4\gamma \\ \cos 3\gamma & \sin 3\gamma & \cos 6\gamma & \sin 6\gamma \\ \cos 4\gamma & \sin 4\gamma & \cos 8\gamma & \sin 8\gamma \end{bmatrix} \begin{bmatrix} i_{s\alpha} \\ i_{s\beta} \\ i_{sx} \\ i_{sy} \end{bmatrix} \tag{16}$$

REFERENCES

[1] F. Wilczynski, P. Strankowski, J. Guziński, M. Morawiec, and A. Lewicki, "Sensorless field oriented control for five-phase induction motors with third harmonic injection and fault insensitive feature," *Bulletin of the Polish Academy of Sciences Technical Sciences*, vol. 67, no. No. 2, pp. 253–262, 2019. [Online]. Available: http://journals.pan.pl/Content/112188/PDF/11_253-262_00847_Bpast.No.67-2_06.02.20.pdf

[2] A. G. Yepes, D. S. Fonseca, H. R. Antunes, O. Lopez, A. J. M. Cardoso, and J. Doval-Gandoy, "Discrimination between eccentricity and interturn faults using current or voltage-reference signature analysis in symmetrical six-phase induction machines," *IEEE Transactions on Power Electronics*, vol. 38, pp. 2421–2434, 2 2023.

[3] G. Kulandaivel, E. Sundaram, M. Gunasekaran, and S. Chenniappan, "Five-phase induction motor drive-a comprehensive review," *Frontiers in Energy Research*, vol. 11, p. 1178169, 8 2023.

[4] P. Drozdowski, "Speed control of multiphase cage induction motors incorporating supply sequence," *Archives of Electrical Engineering*, vol. vol. 63, no. No 4 December, pp. 511–534, 2014. [Online]. Available: http://www.journals.pan.pl/Content/84988/PDF/01_paper.pdf

[5] K. Teler, M. Skowron, and T. Orłowska-Kowalska, "Verification of mlp network-based current sensor fault classifier for vector-controlled ac motor drives," *Bulletin of the Polish Academy of Sciences Technical Sciences*, vol. 72, no. 6, p. e150336, 2024. [Online]. Available: http://journals.pan.pl/Content/131303/PDF/BPASTS_2024_72_6_4295.pdf

[6] P. Zhu, M. Qiao, Y. Wei, and Y. Xia, "Research on five-phase induction motor system control with third harmonic current injection," *The Journal of*

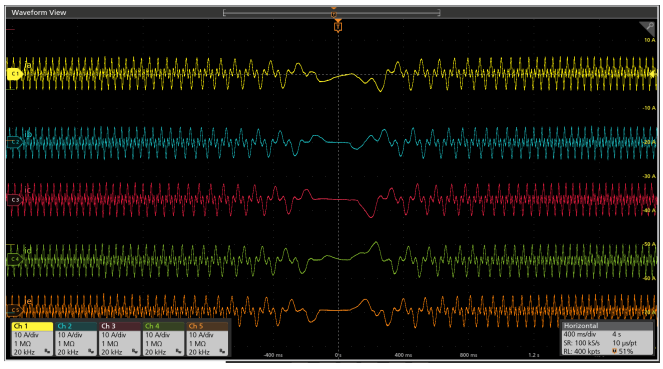

Fig. 14. Stator current waveform for motor reversal procedure in the range of 750 to -750rpm, measured results.

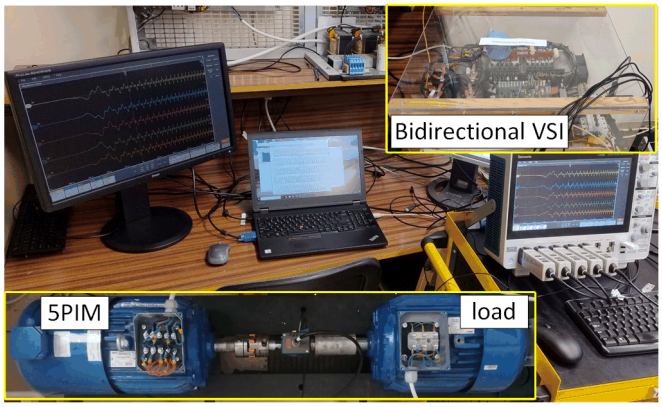

Fig. 15. The view of a test stand-up with a bidirectional voltage source converter, electric drive and multi-channel oscilloscope.

Table 1. Five-phase Induction Motor Parameters

symbol	Parameter	Value
P_n	IM nominal power	5.5kW
ω_n	Rated speed	1420 rpm
I_n	Rated current	8.8
f_n	Rated stator frequency	50Hz
$R_s^{(1)}$	Stator resistance 1stplane	1.04 Ω
$R_r^{(1)}$	Rotor resistance 1stplane	1.69 Ω
$L_s^{(1)}$	Stator leakage inductance 1stplane	11mH
$L_r^{(1)}$	Rotor leakage inductance 1stplane	11mH
$L_m^{(1)}$	Magnetization inductance 1stplane	286mH
$R_s^{(2)}$	Stator resistance 2ndplane	1.04 Ω
$R_r^{(2)}$	Rotor resistance 2ndplane	2.56 Ω
$L_s^{(2)}$	Stator leakage inductance 2ndplane	9mH
$L_r^{(2)}$	Rotor leakage inductance 2ndplane	9mH
$L_m^{(2)}$	Magnetization inductance 2ndplane	48mH

Engineering, vol. 2017, pp. 2559–2563, 1 2017. [Online]. Available: https://onlinelibrary.wiley.com/doi/full/10.1049/joe.2017.0789https://onlinelibrary.wiley.com/doi/abs/10.1049/joe.2017.0789https://ietresearch.onlinelibrary.wiley.com/doi/10.1049/joe.2017.0789

[7] H. Chen, J. Zhao, H. Wang, Q. Zhang, X. Luo, H. Xu, and Y. Xiong, "Multi-objective optimum design of five-phase squirrel cage induction motor by differential evolution algorithm," *Energy Reports*, vol. 8, pp. 51–62, 2022, the 2022 International Conference on Energy Storage Technology and Power Systems. [Online]. Available: https://www.sciencedirect.com/science/article/pii/S2352484722018224

[8] S. Fan, D. Meng, and M. Ai, "Efficiency analytical of five-phase induction motors with different stator connections for fracturing pump drives," *Energy Reports*, vol. 8, pp. 405–413, 2022. [Online]. Available: https://www.sciencedirect.com/science/article/pii/S2352484721013846

[9] H. Liu, J. Wang, and Z. Zhang, "Performance analysis of variable speed multiphase induction motor with pole phase modulation," *Archives of Electrical Engineering*, vol. vol. 65, no. No 3 September, pp. 425–436, 2016. [Online]. Available: http://journals.pan.pl/Content/102150/PDF/DOI%2010.1515aee-2016-0031.pdf

[10] C. Jedryczka, M. Mysinski, and W. Szelag, "Development and analysis of six-phase synchronous reluctance motor for increased fault tolerance capabilities," *Energies 2024, Vol. 17, Page 2351*, vol. 17, p. 2351, 5 2024. [Online]. Available: https://www.mdpi.com/1996-1073/17/10/2351/htmhttps://www.mdpi.com/1996-1073/17/10/2351

[11] J. Laksar, R. Cermak, and K. Hruska, "Challenges in the electromagnetic design of multiphase machines: Winding and equivalent circuit parameters," *Energies*, vol. 14, no. 21, 2021. [Online]. Available: https://www.mdpi.com/1996-1073/14/21/7335

[12] J. Listwan and K. Pieńkowski, "Field-oriented control of five-phase induction motor with open-end stator winding," *Archives of Electrical Engineering*, vol. vol. 65, no. No 3 September, pp. 395–410, 2016. [Online]. Available: http://journals.pan.pl/Content/102148/PDF/DOI%2010.1515aee-2016-0029.pdf

[13] M. Rolak, M. Malinowski, and H. Che, "Modelling and fault-tolerant control of 5-phase induction machine," *Bulletin of the Polish Academy of Sciences Technical Sciences*, vol. 63, no. No 4, pp. 997–1006, 2015. [Online]. Available: http://journals.pan.pl/Content/84391/PDF/20_paper.pdf

[14] L. Sienkiewicz, F. Wilczynski, and S. Racewicz, "Stand-alone operation of multi-phase doubly-fed induction generator supplied by sic-based current source converter," *Energies*, vol. 18, no. 11, 2025. [Online]. Available: https://www.mdpi.com/1996-1073/18/11/2753

[15] K. Saad, K. Abdellah, H. Ahmed, and A. Iqbal, "Investigation on svm-backstepping sensorless control of five-phase open-end winding induction motor based on model reference adaptive system and parameter estimation," *Engineering Science and Technology, an International Journal*, vol. 22, no. 4, pp. 1013–1026, 2019. [Online]. Available: https://www.sciencedirect.com/science/article/pii/S221509861831437X

[16] H. Liu, D. Wang, X. Yi, X. Zheng, X. Yu, and B. Pan, "Loss reduction of five-phase induction motor with third harmonic injection throughout widest torque range under open-circuit faults," *IEEE Journal of Emerging and Selected Topics in Power Electronics*, vol. 11, no. 5, pp. 4643–4658, 2023.

[17] D. Vyas, S. Ibn Islam Joy, M. Morawiec, G. Kostro, L. Sienkiewicz, and N. Joshi, "Sensorless control with multi-scalar transformation of five-phase ipmsm," *Bulletin of the Polish Academy of Sciences Technical Sciences*, vol. 73, no. 4, p. e154281, 2025. [Online]. Available: http://journals.pan.pl/Content/135062/PDF/BPASTS_2025_73_4_4709.pdf

[18] R. Ryndzionek, K. Blecharz, F. Kutt, M. Michna, and G. Kostro, "Development and performance analysis of a novel multiphase doubly-fed induction generator," *Archives of Electrical Engineering*, vol. vol. 71, no. No 4, pp. 1003–1015, 2022. [Online]. Available: http://journals.pan.pl/Content/125038/PDF/art12_int.pdf

[19] M. Korkosz, A. Młot, E. Sztajmec, and K. Ryłło, "Analysis of the impact of the method of manufacturing a rotor on the parameters of an ac ipm machine," *Bulletin of the Polish Academy of Sciences Technical Sciences*, vol. 73, no. 4, p. e153433, 2025. [Online]. Available: http://journals.pan.pl/Content/134027/PDF-MASTER/BPASTS_2025_73_4_4692.pdf

[20] M. Bermúdez, F. Barrero, C. Martín, and M. Perales, "Performance analysis of direct torque controllers in five-phase electrical drives," *Applied Sciences*, vol. 11, no. 24, 2021. [Online]. Available: https://www.mdpi.com/2076-3417/11/24/11964

[21] P. Strankowski, J. Guzinski, M. Morawiec, A. Lewicki, and F. Wilczynski, "Sensorless five-phase induction motor drive with third harmonic injection and inverter output filter," *Bulletin of the Polish Academy of Sciences: Technical Sciences*, vol. 68, pp. 437–445, 6 2020.

[22] K. Blecharz, R. Ryndzionek, P. Gondran, and I. Merzouk, "Slip compensation technique in five-phase induction motors drive system," *Bulletin of the Polish Academy of Sciences Technical Sciences*, vol. 73, no. 4, p. e153223, 2025. [Online]. Available: http://journals.pan.pl/Content/133610/PDF/BPASTS-04685-EA.pdf